Title: Uniform Ni particles on amino-functionalized SBA-16 with excellent activity and stability for syngas methanation

Author: Zhicheng Bian Xin Meng Miao Tao YuHao Lv Zhong Xin

PII: S1381-1169(16)30095-4
DOI: http://dx.doi.org/doi:10.1016/j.molcata.2016.03.028
Reference: MOLCAA 9827

To appear in: *Journal of Molecular Catalysis A: Chemical*

Received date: 4-12-2015
Revised date: 23-2-2016
Accepted date: 16-3-2016

Please cite this article as: Zhicheng Bian, Xin Meng, Miao Tao, YuHao Lv, Zhong Xin, Uniform Ni particles on amino-functionalized SBA-16 with excellent activity and stability for syngas methanation, Journal of Molecular Catalysis A: Chemical http://dx.doi.org/10.1016/j.molcata.2016.03.028

Uniform Ni particles on amino-functionalized SBA-16 with excellent activity and stability for syngas methanation

Zhicheng Bian[1]，Xin Meng[1,2]，Miao Tao[1]，YuHao Lv[1] and Zhong Xin[1,2]*

[1]Shanghai Key Laboratory of Multiphase Materials Chemical Engineering,

[2]State Key Laboratory of Chemical Engineering, School of Chemical Engineering, East China University of Science and Technology, Shanghai, People Republic of China

***Information for Corresponding author**

Name: Zhong Xin

E-mail address: xzh@ecust.edu.cn.

Tel: +86-021-64251005; Fax: +86-021-64240862

Address: No.130 Meilong Road, Xuhui District, Shanghai, China.

Graphic abstract

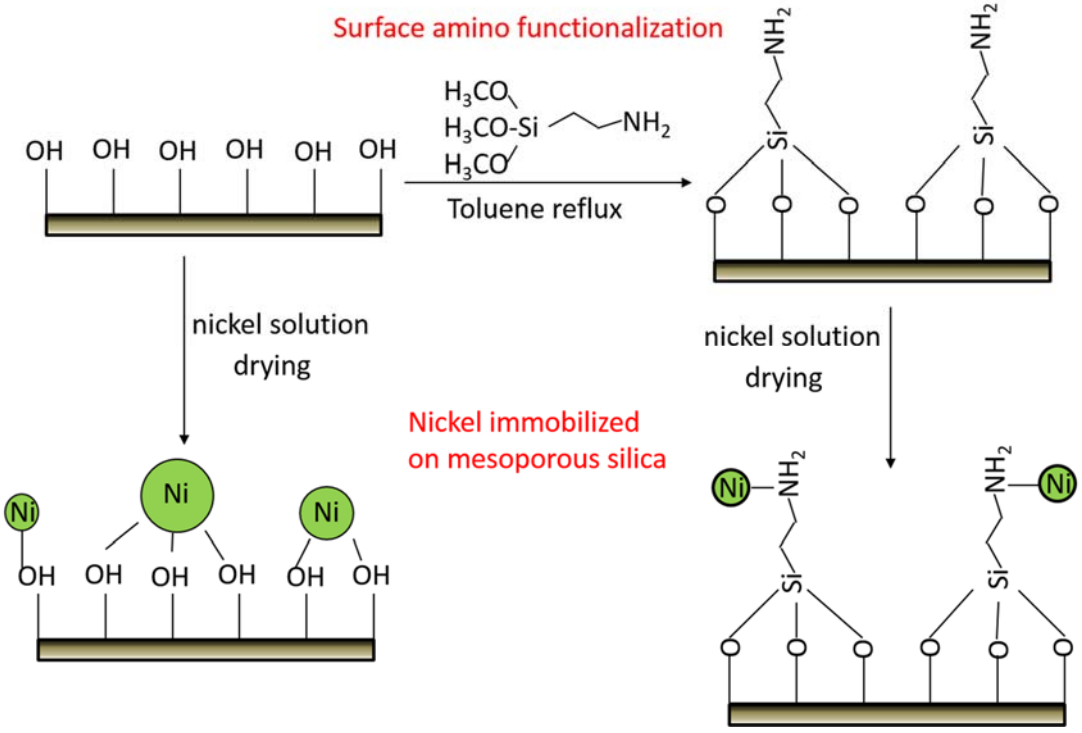

Highlights：

- Amino-functionalized mesoporous material SBA-16 was prepared by silylation.
- Uniform size of nickel particles were observed on the modified material.
- Better thermalstability and long-term stability was achieved for Ni/SBA-16-NH_2 catalyst.

Abstract:

Via modification of mesoporous material SBA-16 with silane coupling agent, a new functionalized SBA-16 catalyst immobilized Ni has been prepared. The performance of the

catalyst for CO methanation then were systemically investigated in a continuous flow fixed-bed reactor. The as-synthesised catalyst was characterized with N_2 absorption-desorption, X-ray diffraction, Transmission electron microscopy (TEM), FT-IR spectrum, ^{29}Si-nuclear magnetic resonance (NMR), H_2 -Temperature Programmed Reduction (TPR) and H_2 pulse chemisorption. After modification by aminopropyl-trimethoxysilane (APTMS), the internal surface silanol group of support SBA-16 was replaced by amino-groups. The replacement of hydroxyl groups by amino groups could prevent the agglomeration of metal ion in the solution. Also uniform nickel particle size was observed because the replaced organic groups on SBA-16 could form homogeneous interaction towards the metal. Comparing with the catalyst without functionalized, the catalyst Ni/SBA-16-NH_2 exhibited higher activity, excellent heat-resistant performance and better stability in CO methanation. The CO conversion and CH_4 selectivity could be 100% and 99.9% at the optimal temperature. Meanwhile, the catalyst showed no decrease of activity in the 100 h life test.

Keyword: amino-functionalized, SBA-16, uniform particle size, CO methanation

1. Introduction

Natural gas, a clean and efficient energy, has received more attention due to its high caloric value and environmental friendlessness[1]. In recent years, due to the rise of natural gas price, the wish for less dependency on natural gas import, and replacement of oil products, synthetic or substitute natural gas (SNG) production from renewable or syngas from coal is attracting attention in some developing countries. Among different fossil fuels, natural gas that consists primarily of methane is ideal, owing to its ready availability, high energy density and conversion efficiency.

Meanwhile, natural gas can be transported efficiently at low cost using existing natural pipelines. Therefore, coal to natural gas(SNG) has been investigated deeply because of the " rich in coal, poor in oil and natural gas" energy landscape in China[2]. And recently severe environmental problems occurred in China due to the combusting of coal. In this situation, coal to synthetic natural gas (SNG) has attracted more and more attention. CO methanation reaction is one of the key reactions in the coal-to-SNG process and the catalyst design is the hard core of the reaction. Therefore, it would be worthwhile to develop an efficient catalyst for the methanation reaction. For the production of SNG, the CO methanation ($CO+3H_2=CH_4+H_2O$) is a key reaction which is highly exothermic and thermodynamically feasible[3]. Due to the property of the reaction, catalysts with high activity and stability in high temperature is of vital importance.

Generally, nickel-based catalyst has been widely employed in CO methanation because of its low price and relatively high activity. However, poor stability caused by carbon deposition and aggregation of active nickel in high temperature limited the industrial application [4; 5]. Therefore, development of catalyst with high activity and excellent stability is the purpose of the research. In previous work, it is found that SBA-16 was a good support to impregnation metal species because it has large surface area, tunable cage size (4-10 nm) and interconnected nanocage[6]. However, the catalyst prepared by SBA-16 revealed poor stability at high temperature. In order to solve the problem, one solution is to select a promoter metal such as Mo, Ce, Mg and Pt to produce a synergistic effect with Ni, which was investigated deeply in recent research [3; 7-10].However, the introduction of the noble metal may cause an environmental problem, which was difficult for recycle. Another popular method to improve the stability of catalyst is the modification of the support [11-13]. Recently, induction of organo-functional groups to ordered mesoporous silica by

silylation have achieved more attention in many fields, such as catalysis, separation and absorption [14-17]. After silylation by organosilanes such as aminopropyl-trimethoxysilane (APTMS), the hydrophobic and hydrophilic nature of mesoporous silica surface was drastically changed, because the hydrophilic silanol group was replaced by hydrophobic chloroalkyl chains through silylation. Jianwen Wei et al found that amino-functionalized SBA-16 showed high hydrothermal stability and thermal stability comparing with SBA-16[18]. Via modification of mesoporous material SBA-16 followed by absorption of $Pd(OAC)_2$, the catalysts exhibited excellent activity and recyclability for the aerobic oxidation of alcohols in water[19]. Hengquan Yang also prepared a novel catalyst by immobilizing Pd and guanidine on the mesoporous materialSBA-16 via a one-pot silylation and found the catalysts showed better activity for Suzuki coupling and the aerobic oxidation of alcohols[19]. It is concluded modification with support by silylation may improve the property of catalyst and enhance the stability of as-prepared catalysts.

This work aims to prepare a more stable catalyst for CO methanation. By grafting the amino group onto the surface of mesoporous material SBA-16 by silylation and followed the impregnation of Ni, we have successfully synthesized the Ni/SBA-16-NH_2 catalysts. The behavior of the prepared catalysts for CO methanation was also investigated and discussed.

2. Experimental Section

2.1. Synthesis

SBA-16 was synthesized according to published methods[6; 20]. Typically, 2.5 g Pluronic F127 (Aldrich) and 15g K_2SO4 was dissolved in 150mL of a 2.0M HCl aqueous solution. After stirring at 38℃ for 2 h, 12g tetraethoxysilane (TEOS, Wako, 95%) was then added to this solution. The molar ratio of TEOS/F127/HCl/ K_2SO4/H_2O was controlled at 1/0.0035/1.5/6/166. The

obtained mixture was vigorously stirred at 38℃ for 24 h. The mixture is then aged at 100℃ for 24 h under static conditions. The solid product was filtered, washed with distilled water and dried overnight at 70℃. Finally the template F127 was removed by calcination at 550℃ for 6 h.

In general, the functionalization of SBA-16 were obtained by post-synthesis grafting methods[21].Typically,1 g of SBA-16(evacuated at 125 □ for 6 h) was dispersed in 50mL of dry tolune. Then 2~4 g aminopropyl-trimethoxysilane(APTMS) was added into the solution. After stirring for 12h at 110□ under a N_2 atmosphere. The resulting solid was isolated by a filtration, washed by tolune and ethanol three times and dried under vacuum overnight to give SBA-16-NH_2.

Ni/SBA-16-NH_2 catalysts were prepared by incipient wetness impregnation. In previous work, it was found that 10wt% Ni content was optimally for the reaction. Typically, SBA-16-NH_2 (1.0g) was added into an aqueous mixture (1.35mL) of Ni $(NO_3)_2 \cdot 6H_2O$ (Wako, 99.9%). The prepared catalysts were denoted as Ni/SBA-16-NH_2. In addition, a reference Ni/SBA-16 catalysts were prepared by wet-impregnation method with the same nickel content of 10%wt.

2.2Characterization

FT-IR spectra were recorded on a Nicolet NEXUS 670 FT-IR spectrometer with a DTGS detector, and samples were measured with KBr pellets. Solid-state ^{29}Si magic angle spinning (MAS) NMR spectra were collected on a Varian INOVA 600 MHz instrument. Samples were spun in 3.2 mm zirconia rotors at 7 kHz. Typical ^{29}Si MAS NMR parameters were 4000 scans, a 90° pulse length of 5 μs, and a delay of 5 s between scans.

Powder X-ray diffraction (XRD) patterns were recorded on a Bruker advanced D8 powder X-ray diffractometer (Cu K_α, λ=1.5418 Å, 40KV, 40mA). The small angle scan ranges were 0.5-10°with steps of 0.02°and 0.1s for each step. Nitrogen adsorption isotherms were measured at

-196℃ using a physisorption analyzer (ASAP 2020, Micromeritics). Samples were degassed at 200℃ for 2 h prior to adsorption measurements. Specific surface area (S_{BET}) was tested from nitrogen adsorption data in the relative pressure range from 0.05 to 0.20 using the Brunauer−Emmett−Teller (BET) method. Total pore volume (V_t) was estimated from the amount of adsorbed nitrogen at a relative pressure of 0.99.The pore size distribution (PSD) was analyzed by using the nonlocal density functional theory (NLDFT) method considering the adsorption branch of the isotherm, which was performed using an Autosorb-1-C software (Quantachrome Inc.). H_2 temperature-programmed reduction (H_2-TPR) was carried out on a TP-5000 type multifunction adsorption instrument (AutoChem II 2920) in a temperature range from room temperature to 900°C with a heating rate of 10°C min^{-1} in a binary gas flow (10 vol % H_2/Ar) of 30 mL min^{-1} and GC-4000A chromatograph thermal conductivity detector recorded the signal. H_2 pulse chemisorption (Micromeritics AutoChem II 2920) was carried out at 40℃ to investigate the dispersion and metallic surface area of nickel metal in the reduced catalyst. The catalyst sample was pretreated in He for 1h at 200℃. After cooling to room temperature in Ar, 10%H_2/Ar pulse adsorption was performed at 40℃ for 10 times. Thermo gravimetric and differential thermal analysis (TG-DTA) of the catalysts after reaction was conducted on a Netzsch Model STA PC thermo analyzer in a temperature range of room temperature to 900 °C at a heating rate of 10 °C min^{-1} in air flow

2.3 Catalytic Performance

The evaluation of Ni catalysts for CO methanation was carried out in a continuous flow fixed-bed reactor with a stainless steel tube (length, 40 cm; inner diameter, 10 mm). The catalyst (0.4g) diluted with 2.5 g of quartz was filled into the reactor and reduced in situ at 500□ for 2 h in

a continuous flow of pure H_2 (50mL/min). Finally, it was tested over a temperature range of 250-500□. The mixed reactant gas consisted of CO/H_2/N_2 with a molar of 3:1:1, in which N_2 was added as an internal standard gas for GC analysis. Gas hourly space velocity (GHSV, mL (gas)/g (catalyst) ·h) was selected to be15000 except for specific clarification. The outlet gas stream was cooled by a cold water trap and analyzed online by gas chromatography (Techcomp, GC7890T). The amounts of H_2, N_2, CH_4, and CO in the outlet gas were analyzed by a thermal conductivity detector (TCD), while CO_2, C_2H_4, C_2H_6, C_3H_6, and C_3H_8 were analyzed by another TCD with a Plot Q column. The calculation formulas were described as equations (1)-(2):

CO conversion:

$$X_{CO}(\%) = \frac{V_{CO,in} - V_{CO,out}}{V_{CO,in}} \times 100 \quad (1)$$

CH_4 selectivity:

$$S_{CH_4}(\%) = \frac{V_{CH_4,out}}{V_{CO,in} - V_{CO,out}} \times 100 \quad (2)$$

3. Results and discussion

3.1 Characterization of the samples

For amino-functionalized materials, it was significant to confirm the success in grafting amino groups the surface and detect the amount of silanol groups available. The FT-IR spectra in Figure.1 can provide an evidence for amino functionalization on the SBA-16. For two samples, typical Si-O-Si bands of inorganic framework were presented: symmetric vibration around 800 cm-1and asymmetric stretching vibration around 1089 cm-1. Comparing to SBA-16, SBA-16-NH_2 obviously exhibited two additional peaks at 2920 cm^{-1} attributed to the vibrations of C-H in aminopropyl group and 1560 cm^{-1} related to the asymmetric bending of NH_2[11; 14; 19; 22].

The Si MAS NMR spectra of the SBA-16 and amino-functionalized SBA-16 were shown in

Figure 2.For the support before and after amino-functionalized, two peaks at -101and -111ppm were referred to Q^3 and Q^4 peaks, respectively, indicating the presence of $HOSi(OSi)_3$ and $Si(OSi)_4$ species in the silicate framework. After modification by APTMS, the support exhibited two new peaks at -60 and -65ppm, which were assigned to the T^2 and T^3 silicon environment [18; 21; 23]. These two peaks were corresponded to $RSi(OSi)_2(OH)$ and $RSi(OSi)_3$, respectively, revealing the successful silylation of amino-groups onto the support. The $-NH_2$ loading was evaluated to be 1.89 mmol by CHNS elemental analysis. TG analysis was used to investigate the thermal stability of SBA-16-NH_2 and the result was shown in Figure 3. A slight mass loss of 2% was of observed under 120℃,which was attributed to the physically absorbed water. Besides, a major weight loss of 5% between 300-400℃ occurred due to the decomposition of amino groups, suggesting the successful silylation of amino-groups onto the support. The TGA analysis indicated that the amino groups were chemically bonded to the surface of SBA-16 and exhibit a relatively high stability.

Powder X-ray diffraction patterns of as-synthesized samples were shown in Figure 4a.The small angle XRD patterns showed two samples both exhibited the characteristic diffraction peaks of cubic Im3m phase. A strong intensity reflection in $2\theta=0.8°$ and other low intensity reflection at 1.2°, which was corresponded to(110) and (200) planes[24]. According to the results, it was established that functionalization with amino groups of SBA-16 did not reduce the mesoscopic order. Figure 3b showed the N_2 absorption-desorption isotherms of SBA-16, SBA-16-NH_2 and Ni/SBA-16-NH_2. The calculated texture properties of the samples were listed in Table 1. It can be seen in Figure 4b that SBA-16 exhibited a type-IV isotherm pattern with an H2 hysteresis loop in the relative pressure of 0.4-0.7,which was confirmed as a mesoporous cage-like structure[25].

Comparing to the reference material SBA-16, SBA-16-NH_2 also showed the type-IV isotherm pattern with an H2 hysteresis loop, indicating that the material after modification still remain the mesostructure. However, it was found that the N_2 adsorption-desorption volume decrease a lot, which corresponded to the decrease of pore volume of SBA-16-NH_2 revealed in Table 1. Also in Figure 4c, the pore size of SBA-16-NH_2 decreased from 6.9nm to 4.9nm. This may be due to the stereo-hindrance effect after the amino group grafted on the internal surface of the support. It was also proved that almost hydroxyl groups on the internal surface was replaced by amino-groups. It was worth noting that adsorption and desorption curve didn't closed in the range of p/p_0=0-0.3 for SBA-16-NH_2. Such phenomenon may be the results of the decomposition organic group in aminopropyl group and pore blockage formed [22; 26]. After impregnation of Ni $(NO_3)_2$ and the followed calcination, the catalyst maintained the mesoporous cage-like structure with a slight decrease in surface and pore volume.

In order to investigate the influence of APTMS concentration on the support and the catalyst, molar ratio of SBA-16: APTMS was controlled as 0.1, 0.2, 0.4, 0.8. Table 1 listed the texture properties of SBA-16 and SBA-16-NH_2(x), which the x indicated the molar ratio of SBA-16: APTMS. As seen in Table 1, the BET surface area, pore volume did not suffer significant changes between different concentrations of APTMS. Also from the CHNS element analysis, the amount of grafted amino groups has no obvious changes with the increase of APTMS concentration. The wide XRD diffraction(Figure 4d) was used to investigate the average particle size of nickel. In Table 1, the average nickel particle size were calculated by Scherrer's equation and the same trend was found. This suggested that no obvious changes occurred with the increase concentration of APTMS. SBA-16-NH_2 (0.2) was selected for further investigation for catalytic performance.

The structure of the support and the dispersion of the metal species could be obviously speculated from Transmission electron microscopic images. Figure 5 showed the TEM images of the samples. It was revealed in Figure 5a-b that support before and after silylation both exhibited highly ordered arrangement of mesopores, indicating the support after silylation maintained a high-quality body-centered cubic mesostructure. After introduction of nickel species, some shrinkage was suggested to partly occur. The amino-functionalized support obviously improved the nickel dispersion. Ni particles with a much narrow distribution(10nm) was shown in Fig 5f, while the catalyst Ni/SBA-16 exhibited a much wider distribution of nickel particles(Fig 5e).H_2 pulse chemisorption results also indicated the dispersion of nickel increased from 1.54% for Ni/SBA-16 to 1.95% for Ni/SBA-16-NH_2. The impregnation process can be explained like:(i)in the early step, the surface of support has a lot absorbed water, which the ion(Ni^{2+}) was dissolved in;(ii)in the dry step, the surface water evaporated and the ion concentration in the water film was increased and crystal growth formed. For Ni/SBA-16 catalyst, the support surface has much hydroxyl groups and the mutual attraction between hydroxyl groups and absorbed water would take the ion accumulated on the surface, which led the large particle formed. In contrast, the support modified by organic groups reduced or eliminate the hydroxyl groups and exhibited some steric hindrance effect, which would prevent the ions aggregation on the surface. It was also suggested that the surface of the support was modified by amino groups and the metal species could be absorbed in the nanocage of the support and the nickel was not easily accumulated with the evaporation of the solvent in the drying step[11].

Figure 6 showed the H_2-TPR profiles of the unreduced catalysts. It can be seen that catalysts prepared without silylation showed a low temperature reduction peak at 300℃ with a shoulder at

about 500℃,which points out the coexistence in the catalyst of NiO species of different degrees of agglomeration. After the support were functionalized by APTMS, only one well-defined peak with a maximum at 300℃ was observed in the TPR profiles of Ni/SBA-16-NH_2,which the position was corresponded to the reduction of dispersed NiO species. It was interesting to notice that the amino-functionalized support resulted in a more homogeneous distribution of NiO species, which was consistent with TEM images [27].

3.2 Catalytic performance for CO methanation

3.2.1 Activity for CO methanation

In previous section, the activity of Ni/SBA-16 have been deeply investigated. Although the catalyst reveled good performance in activity test, it showed poor performance in heat-resistant and stability test. Thus, the better performance in heat-resistant and stability test with comparable activity with the reference catalyst is the purpose. Figure 7 showed the CO methanation performance of Ni/SBA-16 catalysts at 0.1MPa under 300-500℃. It could be conclude that Ni/SBA-16-NH_2 and Ni/SBA-16 catalyst showed 100% CO conversion in the lower temperature of 300-400℃. Regarding with CH_4 selectivity, it was found that in the whole temperature range the catalyst Ni/SBA-16-NH_2 exhibited better performance than Ni/SBA-16. Also it was found that catalysts exhibited best activity at the temperature range from 300-400℃. It worth noting that at 350℃ catalyst Ni/SBA-16-NH_2 brought out the best activity with ~100% CO conversion and ~99.9% CH_4 selectivity. From TEM images， it was found that the support with amino-functionalized could result in highly uniform metal particle size, which further given rise to the better activity.

3.2.2 Stability of the catalyst

In previous section, it was found that catalysts prepared with amino-functioned SBA-16 exhibited higher activity than Ni/SBA-16. For CO methanation, heat-resistant performance and stability of catalysts is of vital importance. In order to take a deep insight into the influence of support, the heat-resistant performance of catalysts was investigated. The heat-resistant performance was investigated by comparing the activities of catalysts before and after calcination at 700□ in N_2 atmosphere. Firstly, the activities of catalysts were evaluated at 350□ under 0.1MPa, calcined at 700□ for 2h and cooled to 350□ for activities test under the similar situations. The activities of catalysts before and after calcination are shown in table 2.

From table 2, it was found that the activity of Ni/SBA-16 catalyst showed an obvious decline after calcination at 700℃ for 2 h. The CO methanation and CH_4 selectivity decreased from 100% and 96% to 95.2% and 83.7 in N_2 atmosphere. For Ni/SBA-16-NH_2 catalyst, there was no significant decline for the activity after calcination at 700℃ in N_2 atmosphere. Above evaluations revealed that Ni/SBA-16-NH_2 exhibited a better activities Ni/SBA-16 and excellent high-temperature-resistant performance comparing with Ni/SBA-16. In order to understand whether carbon deposition or catalyst sintering is the main reasons leading to the deactivation of the catalysts. TG was carried out in air for the catalysts after calcination and the results was shown in Fig 8. Form the Figure 8, it can be found that with the increasing of temperature, four weight changes were identified over Ni catalysts: water loss(50-100℃), carbon loss(150-300℃), oxidation of metal nickel(300-450℃) and carbon loss(500-800℃), respectively. Therefore, the carbon deposition over the catalysts was the sum of the weight loss at 150-300℃ and 500-750℃. And the amount of carbon deposition was calculated to be 1.2% for Ni/SBA-16-NH_2 and 2.0% for

Ni/SBA-16. The carbon deposition of two catalysts were not in big gap, indicating that the carbon was not the main reason for the deactivation. Meanwhile, a regeneration measurement is carried on. Conventionally, the carbon deposition is removed by air treatment. Since the remove of deposition carbon can be easily achieved at 700℃ and the regeneration of catalysts was carried by treating with air at 700℃. First the catalysts after calcination was treated by air at 700℃ for 4 h. Since the air treatment lead to the formation of NiO and the catalysts is further reduced under H_2 flow at 500℃ for 2 h. The regenerated catalysts were also tested for CO methanation and the results were listed in Table 2. As shown in Table 2, Ni/SBA-16 after generation still exhibit a significant decrease in CO conversion and CH_4 yield, while Ni/SBA-16-NH_2 retained the same activity as before. Thus, combining the TG results and activity test after regeneration, coke formation can be exclude for the reasons of deactivation.

The TEM images of the calcined support and the catalysts were shown in Fig 9a-d. From Fig 9a-b, the well-ordered structure SBA-16 and SBA-16-NH_2 was maintained after calcination at 700 ℃, indicating the good thermal stability of the supports. For Ni/SBA-16 catalyst, a significant agglomeration of nickel particles was found, while uniform nickel species still existed on the surface in Ni/SBA-16-NH_2. When the catalysts calcined at 700℃in gases atmosphere, the catalysts underwent a high temperature reduction and more NiO species reduced. Metallic nickel is easier to sinter at high temperature, leading to form large particle size. Therefore, amino-functionalized support could stabilize the metal particle and remain better activity in harsh reaction conditions.

For CO methanantion, heat-resistant performance and stability of the catalyst is of vital importance in industry. In previous section, it was found that Ni/SBA-16-NH_2 exhibited excellent

heat-resistant performance. The catalytic stability test of Ni/SBA-16-NH_2 was also investigated at 350℃ under atmosphere pressure with a WHSV of 15000 mL/g/h. Figure 10 showed the results of stability test, which CO conversion and CH_4 selectivity are plotted as the function of time. Figure 10a showed the CO conversion of the catalyst in the stability test and it can be seen that CO conversion for two catalysts is maintained at100% without an obvious decline. However, CH_4 selectivity for Ni/SBA-16 decreased from 96% to 89% during a100 h test. In contrast, for Ni/SBA-16-NH_2 catalyst, no obvious decline in CH_4 selectivity was observed.

4. Conclusion

By modification support SBA-16 with silylation, a highly nickel dispersed catalyst was prepared for CO methanation. This catalyst showed high activity for the SNG production with the CO conversion was almost100% and the CH_4 selectivity was 99.9%, respectively. Comparing with the catalyst without modification, a highly dispersion of nickel was found with a much narrow particle size distribution (10nm). The catalyst could retain the high activity without obvious decline after calcination at 700℃ in N_2 atmosphere, which showed excellent behavior in heat-resistant performance. Further, the long-term stability of catalysts were also investigated and catalyst Ni/SBA-16-NH_2 revealed much more stable than Ni/SBA-16.The significantly enhanced stability of the catalyst Ni/SBA-16-NH_2 was attributed to the uniform particle size on the modified surface of the support.

Acknowledgments

This research was financially supported by National Natural Science Funds of China (Grant No. U1203293 and 91434128), the program of Shanghai Subject Chief scientist (Grant No.10Xd1401500) and the Program of Shanghai Leading Talents (2013).

Reference

[1] J. Gao, Q. Liu, F. Gu, B. Liu, Z. Zhong, F. Su, RSC Adv. 5 (2015) 22759-22776.

[2] J.Y. Zhang, Z. Xin, X. Meng, M. Tao, Fuel 109 (2013) 693-701.

[3] D. Hu, J. Gao, Y. Ping, L. Jia, P. Gunawan, Z. Zhong, G. Xu, F. Gu, F. Su, Industrial & Engineering Chemistry Research 51 (2012) 4875-4886.

[4] R.P.W.J. Struis, T.J. Schildhauer, I. Czekaj, M. Janousch, S.M.A. Biollaz, C. Ludwig, Applied Catalysis a-General 362 (2009) 121-128.

[5] S.L. Ma, Y.S. Tan, Y.Z. Han, Journal of Natural Gas Chemistry 20 (2011) 435-440.

[6] Z. Xin, Z. Bian, CN patent 201410239423.9 (2014).

[7] J.Y. Zhang, Z. Xin, X. Meng, Y.H. Lv, M. Tao, Fuel 116 (2014) 25-33.

[8] S. Yagi, A. Kawakami, K. Murase, Y. Awakura, Electrochimica Acta 52 (2007) 6041-6051.

[9] J. Zhang, Z. Xin, X. Meng, Y. Lv, M. Tao, Industrial & Engineering Chemistry Research 52 (2013) 14533-14544.

[10] S. Zhang, S. Muratsugu, N. Ishiguro, M. Tada, ACS Catalysis 3 (2013) 1855-1864.

[11] S. Wei, Z. Ma, P. Wang, Z. Dong, J. Ma, Journal of Molecular Catalysis A: Chemical 370 (2013) 175-181.

[12] H.-b. Wang, Y.-h. Zhang, H.-l. Yang, Z.-y. Ma, F.-w. Zhang, J. Sun, J.-t. Ma, Microporous and Mesoporous Materials 168 (2013) 65-72.

[13] T. Yokoi, Y. Kubota, T. Tatsumi, Applied Catalysis A: General 421-422 (2012) 14-37.

[14] S. Wang, K. Wang, C. Dai, H. Shi, J. Li, Chemical Engineering Journal 262 (2015) 897-903.

[15] J. Sun, Q. Kan, Z. Li, G. Yu, H. Liu, X. Yang, Q. Huo, J. Guan, RSC Adv. 4 (2014) 2310-2317.

[16] X. Xue, F. Li, Microporous and Mesoporous Materials 116 (2008) 116-122.

[17] J. Aburto, M. Ayala, I. Bustos-Jaimes, C. Montiel, E. Terrés, J.M. Domínguez, E. Torres, Microporous and Mesoporous Materials 83 (2005) 193-200.

[18] H. Sun, Q.H. Tang, Y. Du, X.B. Liu, Y. Chen, Y.H. Yang, Journal of Colloid and Interface Science 333 (2009) 317-323.

[19] Z. Ma, H. Yang, Y. Qin, Y. Hao, G. Li, Journal of Molecular Catalysis A: Chemical 331 (2010) 78-85.

[20] C. Yu, B. Tian, J. Fan, G.D. Stucky, D. Zhao, Chemical Communications (2001) 2726-2727.

[21] J. Wei, J. Shi, H. Pan, Q. Su, J. Zhu, Y. Shi, Microporous and Mesoporous Materials 117 (2009) 596-602.

[22] G. Castruita-de León, Y.A. Perera-Mercado, L.A. García-Cerda, J.A. Mercado-Silva, H.I. Meléndez-Ortiz, Y. Olivares-Maldonado, L. Alvarez-Contreras, Microporous and Mesoporous Materials 204 (2015) 156-162.

[23] H.Q. Yang, X.J. Han, Z.C. Ma, R.Q. Wang, J. Liu, X.F. Ji, Green Chemistry 12 (2010) 441-451.

[24] Y.K. Hwang, J.-S. Chang, Y.-U. Kwon, S.-E. Park, Microporous and Mesoporous Materials 68 (2004) 21-27.

[25] E.A. Prasetyanto, Sujandi, S.C. Lee, S.E. Park, Bulletin of the Korean Chemical Society 28 (2007) 2359-2362.

[26] Z. HuiLing, H. Jun, W. JianJun, Z. LiHui, L. HongLai, Acta Physico-Chimica Sinica 23 (2007) 801-806.

[27] T.E. Klimova, D. Valencia, J.A. Mendoza-Nieto, P. Hernandez-Hipolito, Journal of Catalysis 304 (2013) 29-46.

Figure captions:

Figure 1. FT-IR spectra of SBA-16 and SBA-16-NH_2

Figure 2. ^{29}Si solid-state nuclear magnetic resonance of SBA-16(A) and SBA-16-NH_2 (B)

Figure 3. TG and DTA results of the SBA-16-NH_2.

Figure 4. (a) Small-angle XRD patterns of the support and the Ni-catalysts (b) N_2 adsorption-desorption isotherms of the catalysts (c) Pore size distribution of SBA-16 and SBA-16-NH_2

Figure 5. TEM images of samples: (a) SBA-16 (b) SBA-16-NH_2 (c) Ni/SBA-16 (d) Ni/SBA-16-NH_2 with Ni particle size distribution for (e) Ni/SBA-16 (f) Ni/SBA-16-NH_2

Figure 6. H_2-TPR patterns of prepared catalysts

Figure 7. CO methanation properties on Ni catalysts: (a) CO conversion (b) CH_4 selectivity.

Figure 8. Thermogravimetric(TG) results of the catalysts after calcination at 700℃.

Figure 9. TEM images of spent catalysts after calciantion at 700℃:(a)SBA-16(b) SBA-16-NH_2 (c)Ni/SBA-16(d) Ni/SBA-16-NH_2

Figure 10. Catalytic stability of catalysts: (a) CO conversion (b) CH_4 selectivity.

Figure 1

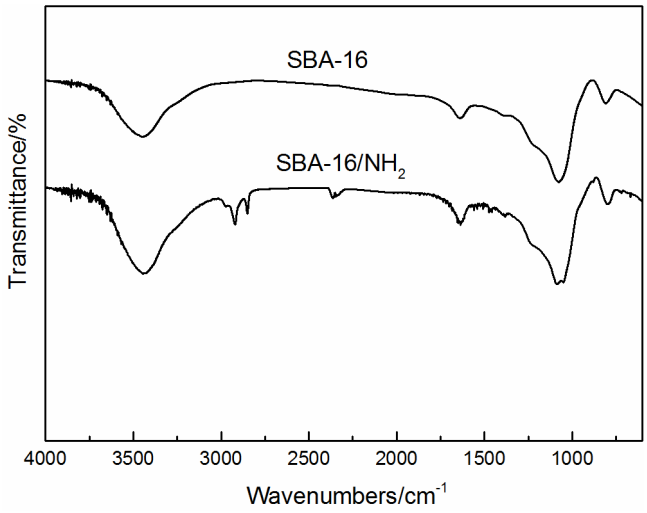

Figure 2

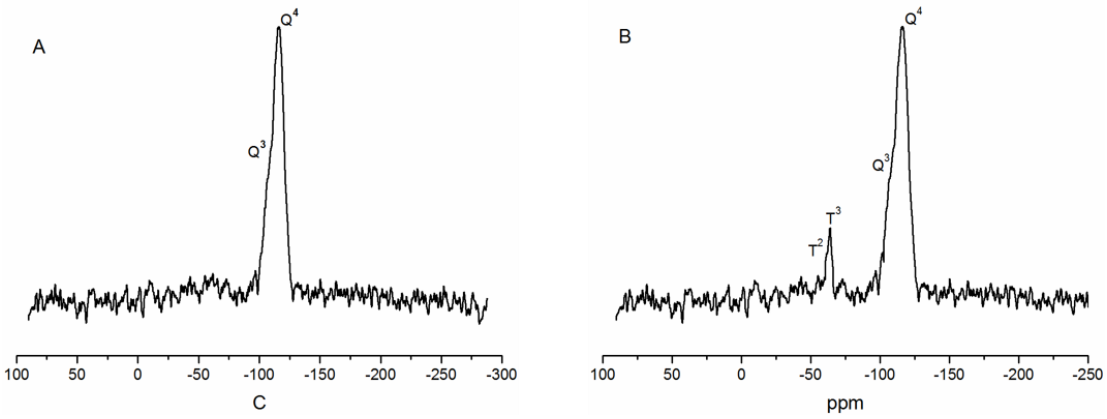

Figure 3

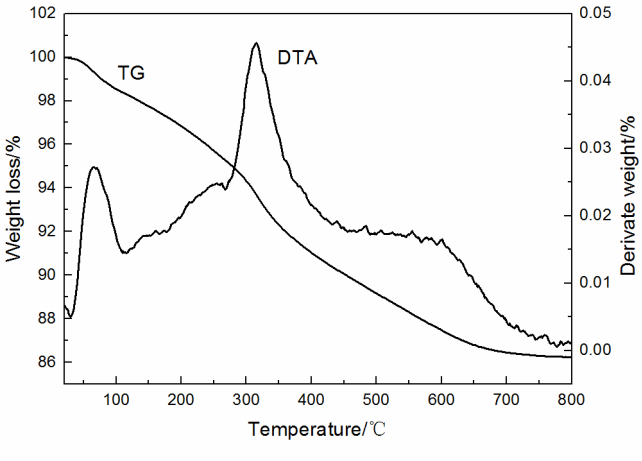

Figure 4

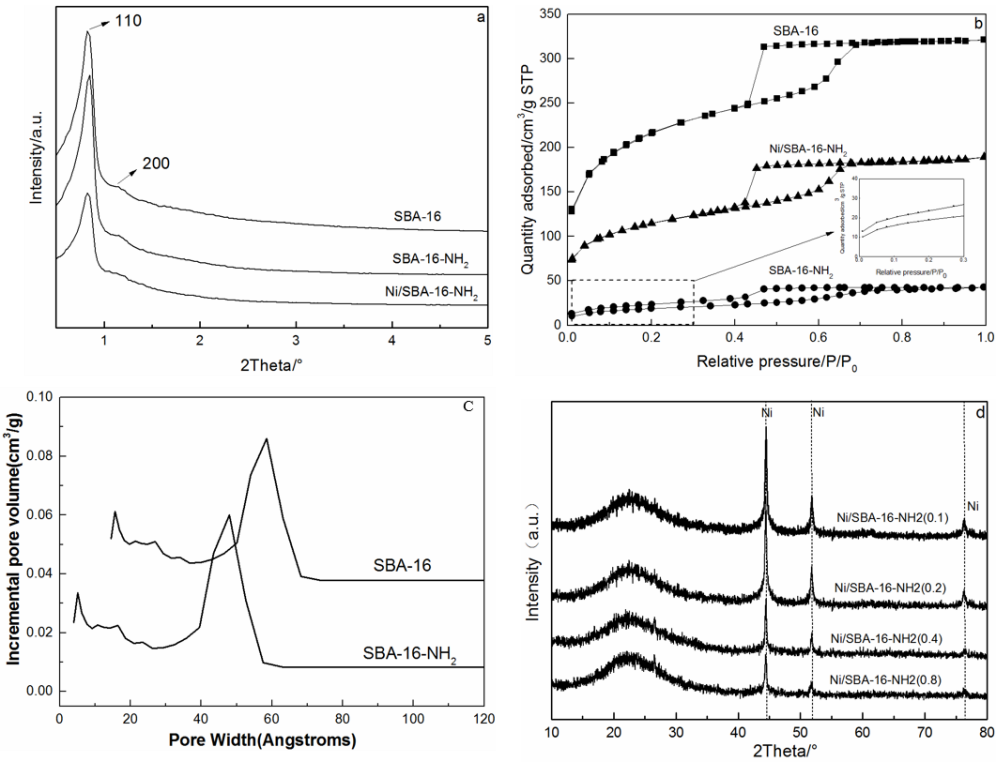

Figure 5

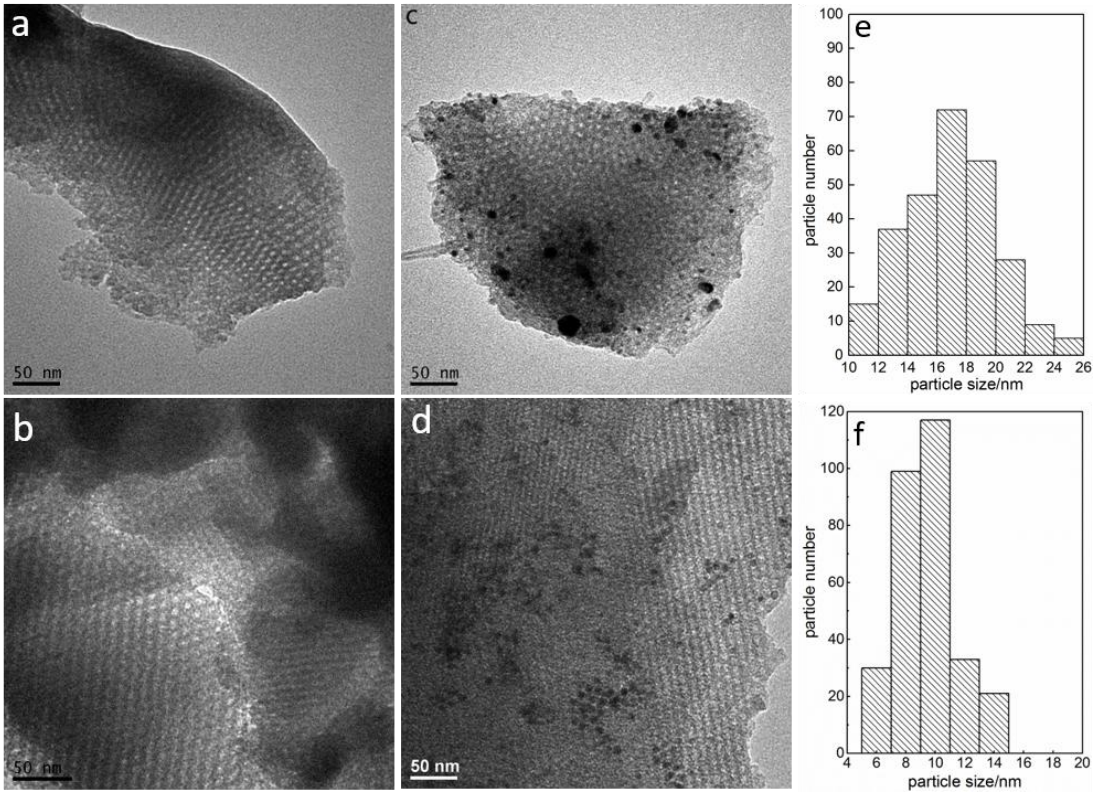

Figure 6

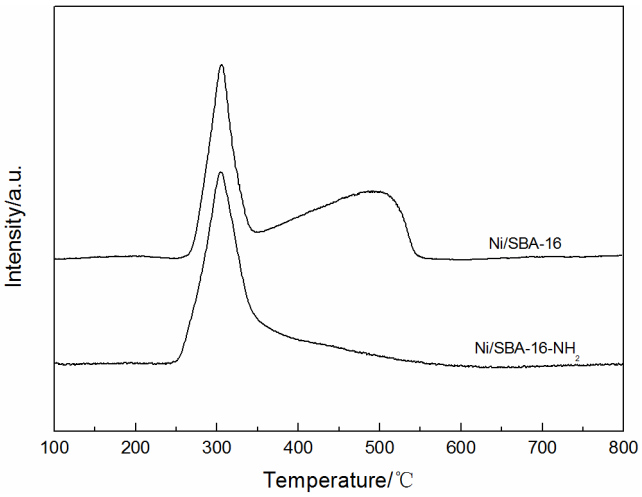

Figure 7

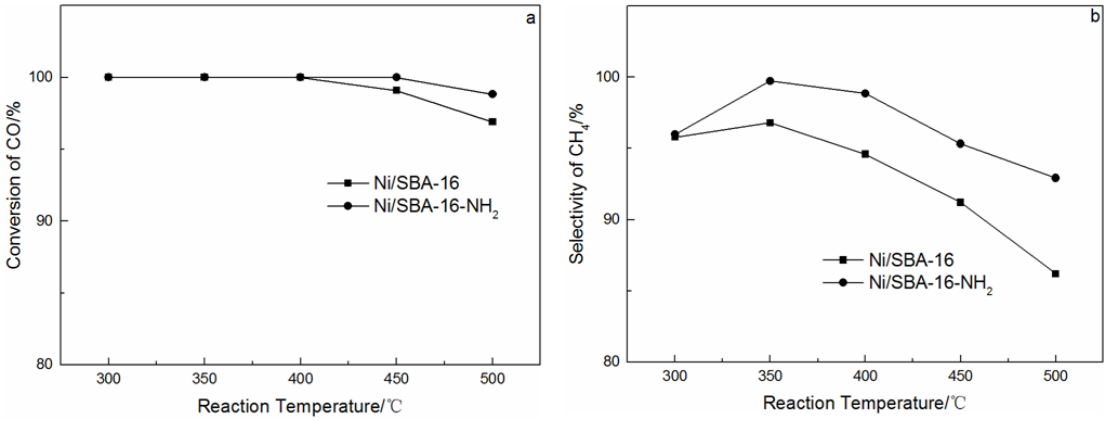

Figure 8

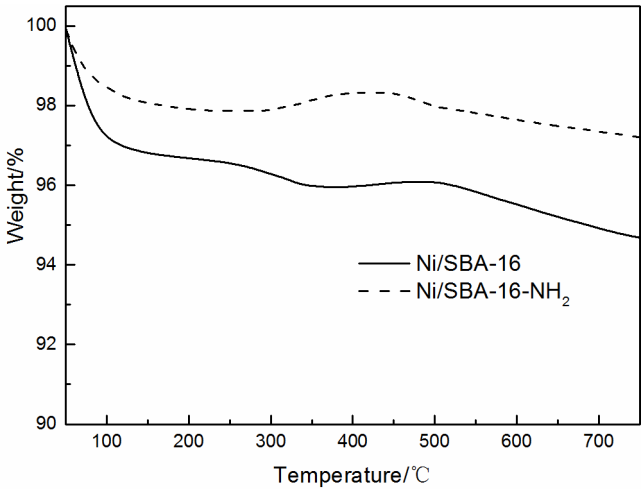

Figure 9

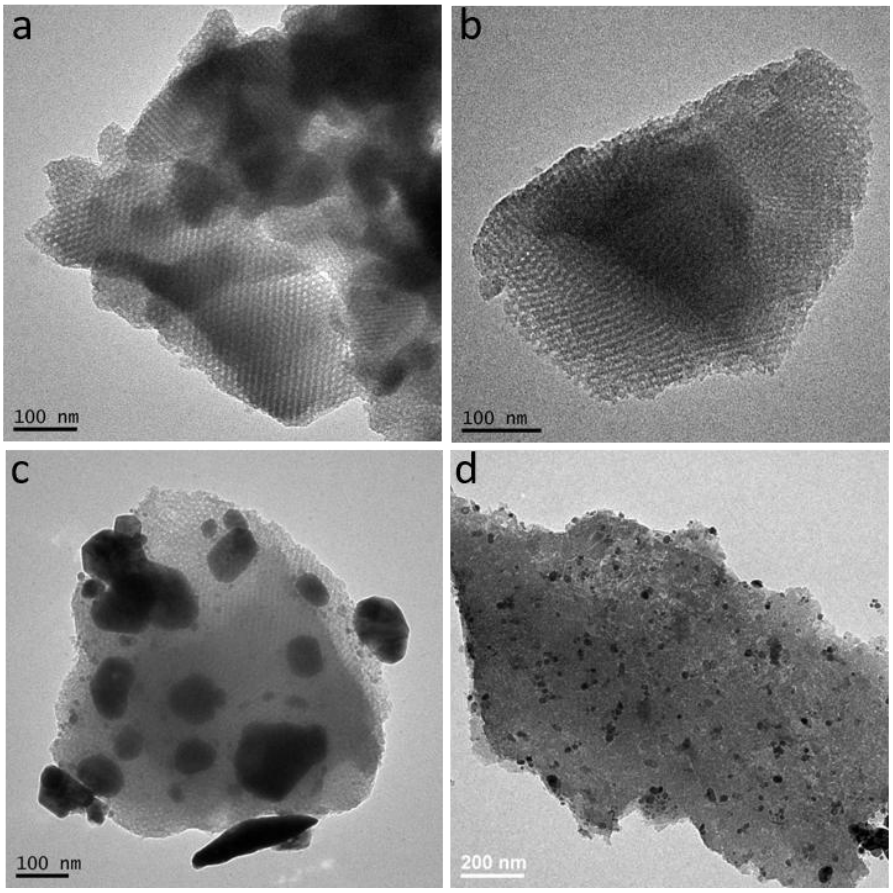

Figure 10

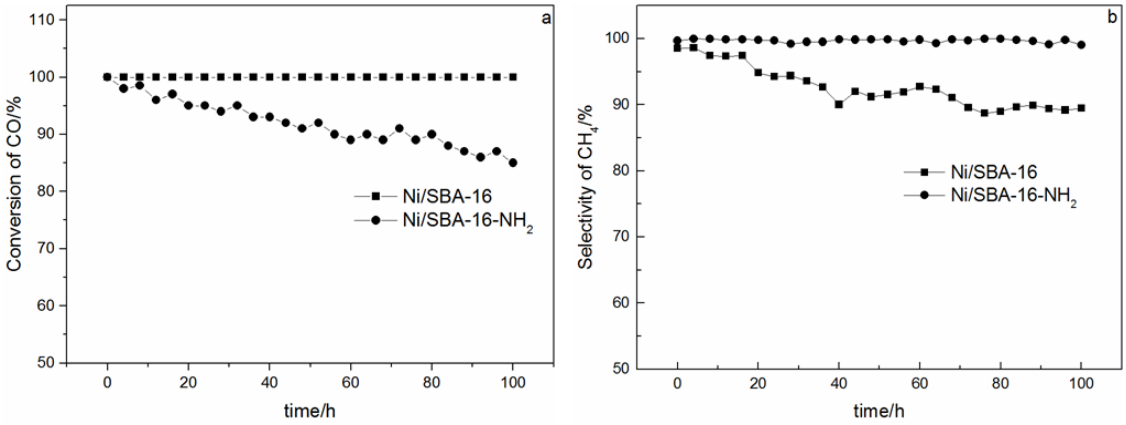

Table 1. Physicochemical Property of the samples

samples	Surface area [a] (m^2/g)	Pore volume [b] (cm^3/g)	Pore size [c] (nm)	Metal crystallite size[d](nm)	Grafted amino groups[e](mmol)
SBA-16	827.7	0.532	6.9	-	-
SBA-16-NH_2(0.1)	70.0	0.068	5.0	15.2	1.75
SBA-16-NH_2(0.2)	68.7	0.064	4.9	13.1	1.85
SBA-16-NH_2(0.4)	65.3	0.063	4.7	14.0	1.86
SBA-16-NH_2(0.8)	63.2	0.061	4.6	14.2	1.89
Ni/SBA-16	490.7	0.350	6.6		
Ni/SBA-16-NH_2(0.2)	570.7	0.361	6.5		

[a] Calculated using BET equation.

[b] Pore volume, obtained from the volume of nitrogen absorbed at P/Po = 0.95.

[c] Calculated by means of the NLDFT method from the absorption branches of the isotherms.

[d] Calculated from Ni(111) plane by Scherrer's equation.

[e] Calculated by CHNS element analysis.

Table 2. Heat-resistant performance of catalysts

Catalyst	Before Calcination		After Calcination		After regeneration	
	C_{CO}/%	S_{CH4}/%	C_{CO}/%	S_{CH4}/%	C_{CO}/%	S_{CH4}/%
Ni/SBA-16	100.0	96.2	95.2	83.7	96.0	85.1
Ni/SBA16-NH_2	100.0	99.9	100.0	99.9	100.0	99.9